Accurate methodology to determine slip velocity, yield stress and the constitutive law for molten chocolate

Emeline Talansier, Audrey Bacconnier, Francois Caton, Carine Chastel, Lucy Costa, Deniz Z Gunes, Denis Christophe D. Roux

Accurate methodology to determine slip velocity, yield stress and the constitutive law for molten chocolate

Emeline Talansier[a,], Audrey Bacconnier[a], François Caton[a], Carine Chastel[a], Lucy Costa[a], Deniz Z. Gunes[b], Denis C.D. Roux[a,*]*

[a]*Univ. Grenoble Alpes, CNRS, Institute of engineering Univ. Grenoble Alpes Grenoble INP, LRP,F-38000 Grenoble, France*

[b]*Nestlé Research Center, Institute of Material Science, Vers-chez-les-Blanc, CH-1000, Lausanne 26, Switzerland*

***Corresponding authors**: emeline.talansier@univ-grenoble-alpes.fr; denis.roux@univ-grenoble-alpes.fr*

Abstract

Flow of concentrated soft materials like molten chocolate often has the ambiguity of behaving like a solid or a liquid depending on the external constraints. Determination of the constitutive law is often unreliable and consequently the yield stress value too. This difficulty of determining yield stress, particularly when using a standards protocol such as the IOCCC for chocolate, is a consequence of the presence of wall slip. Most attempts to assess slip velocity using *Yoshimura and Prud'homme's* method have resulted in failure. We propose to tackle this problem by using an easy and reliable methodology applied to a commercial chocolate in a melted state with, as equipment, a plate-plate rotational rheometer.

This method allows precise determination of the yield stress value, the constitutive law and the slip velocity, as well as also providing an explanation to the apparent Newtonian plateau and thickening behavior of the raw flow curve.

Keywords: Yield stress fluid, Slip velocity, Solid-liquid transition, *Herschel-Bulkley* model, *Casson* model, Molten chocolate

1. Introduction

Molten chocolate, a concentrated suspension of large and solid particles within a continuous fat system, is known to have a non-Newtonian behavior. Sedimentation, wall slip or solid to liquid transition occur in such complex systems (Barnes, 1995; El Kissi et al., 2006) making their rheological characterization difficult although this is essential for the sizing of industrial processes.

However, proper flow characterization is of critical importance for industrial process design, as well as for determining the best adapted formulation window for a given factory process. In the food industry, this is particularly true for chocolate manufacture, since most industrial processes have been optimized since a long time ago. In this context, the International Office of Cocoa, Chocolate and Confectionary office (IOCCC) and the International Chocolate Awards (ICA) organizations have developed specific protocols for molten chocolate (Afoakwa et al., 2009; Beckett, 2000). This protocol, currently accepted as an accepted standard, consists of successive increasing and decreasing shear rate ramps set at a series of values between 2 and 50 s^{-1} (see Table 1a).

Using either a *Casson* or an *Herschel-Bulkley* model, the fit of the experimental data gives the parameters of a constitutive equation (Steffe, 1996). Among these parameters, the yield stress σ_0 below which the material behaves as a solid, is an important parameter difficult to determine. From the IOCCC standard method the following question arises: "Why are only shear rates higher than $2s^{-1}$ used to characterize liquid chocolate?" This is quite surprising since it is

well-known that lower shear rates, below $2s^{-1}$, are today easily attainable with any commercial rheometer.

The answer is certainly hidden within the complex solid to liquid transition of concentrated particles systems for which a resurgence of interest has been seen in the scientific literature (Balmforth et al., 2014; Bonn et al., 2015; Bonn and Denn, 2009; Damianou et al., 2014; Divoux et al., 2011; Grenard et al., 2014; Herzhaft, 2002; Herzhaft et al., 2005; Piau, 2007; Salmon et al., 2003; "Special Issue on Yield Stress Fluids: a 100 Years after Bingham's Landmark Paper," 2017). However, even if our understanding of the solid to liquid transition is gradually improving, few works have been reported on industrial soft condensed matter. Moreover, all the works which have shown interest in solid to liquid transition face the issue of material slip at the solid wall boundaries.

Wall slip velocities are usually quantified by means of capillary rheometry (Mooney, 1931) applied to *Rabinowitsch*-corrected data. Using the same hypothesis as *Mooney*, *Yoshimura and Prud'homme* (Yoshimura and Prud'homme, 1988) developed a fast method based on two sets of experiments to assess wall slip using rotational rheometry. *Yilmazer and Kalyon* (Yilmazer and Kalyon, 1989) generalized this method by applying the Mooney plots procedure to parallel disk geometry and obtained a better value for wall slip velocity. Nonetheless, the *Yilmazer* generalization on rotational rheometry has never been assessed on yield stress fluids with the exception of *Bertola*'s work (Bertola et al., 2003) on aqueous foam and emulsion.

Nevertheless, we should also notice that in liquid chocolate, yield stress determination using the Vane or Couette geometries along with the IOCCC standard method does not take into account the slippage of the material at the wall boundary (Aeschlimann and Beckett, 2000; Afoakwa et al., 2009, 2008; Servais et al., 2003; Sokmen and Gunes, 2006).

In the present paper we present and discuss the applicability of conventional rotational rheometry methods for accurate quantification of wall slip velocity and yield stress determination in a commercial molten chocolate.

2. Materials and methods

2.1. Composition and samples preparation

"Couverture" chocolate containing 64.5% (w/w) cocoa, 27% sugar and 8% fat from the company Barry Callebaut was used. Emulsifier soya lecithin and natural vanilla flavor completed the 0.5% of the remaining components of the mix. This highly fluid chocolate is usually used for molded, coating or tablet use.

Molten chocolate samples were put into a sealed glass bottle which was placed onto a rotating mixer (RM5) inside a Memmert thermostatic chamber (Model UFE 600, 256L). The chamber was maintained at T = 50°C (+/-0.5°C) for a minimum period of two days. This protocol ensured that the chocolate was fully liquid and free of any remaining crystals. This preparation acted as the thermal and sample homogenization step.

2.2. Rheometry

Rheological measurements were performed using an imposed torque rheometer MCR501 (Anton Paar, GmbH) with minimum torque and rotational velocity measures of 0.1 μN.m and 10^{-6} rpm respectively possible. A stainless

steel, smooth plate-plate geometry of 25 mm diameter was employed on the rheometer with different gaps of 0.25, 0.5, 0.75, 1, 1.25, 1.5, 1.6, 1.7 and 1.8 mm. In accordance with the continuum mechanics hypothesis, all gaps were much larger than the largest particles in suspension ($d_{max} \approx 20\mu m$) in this kind of molten chocolate (Beckett, 2000). All measurements were performed at 40°C, using the rheometer's Peltier system. To avoid temporal behavior on creep flow at low stresses, but also aging or complex dynamics induced by residual stresses, thixotropy and retarded viscoelasticity (Benmouffok-Benbelkacem et al., 2010; Caton and Baravian, 2008; Lidon et al., 2017), measurements were conducted by imposing successive increasing and decreasing shear rate ramps as fully described by Table 1b and Fig.1. Increasing shear rate ramps are known to be different from decreasing ones, as illustrated in Fig.1 by the two first ramps of 0 and 5min. Indeed, when passing from solid to liquid state, yield stress fluids may have several different behaviors (Cheddadi et al., 2012; Saramito, 2007) that make the exploitation of increasing ramps impossible. Increasing ramps were only used to fluidize material and the point settings were therefore fewer than those of the decreasing ramps. If compared with the standards presented in Table 1a, the proposed decreasing ramps attained lower shear rates, as low as $0.005s^{-1}$, thus permitting an accurate determination of the constitutive law parameters.

Table 1 *(a) IOCCC2000 and ICA standards.*
(b) Rheometrical protocol and corresponding time sequences.

	Pre-shear	Increasing shear rate	Constant high shear rate	Decreasing shear rate
IOCCC 2000	$5s^{-1}$ on 500s	2 to $50s^{-1}$ on 180s	$50s^{-1}$ on 60s	50-$2s^{-1}$ on 180s
ICA	$5s^{-1}$ on 300s			

(a)

Shear rate (s^{-1})	0.05-50	50-0.005
Number of collected data	16	41
Time (s)	50s / variable	50s / variable from 15 to 50s

(b)

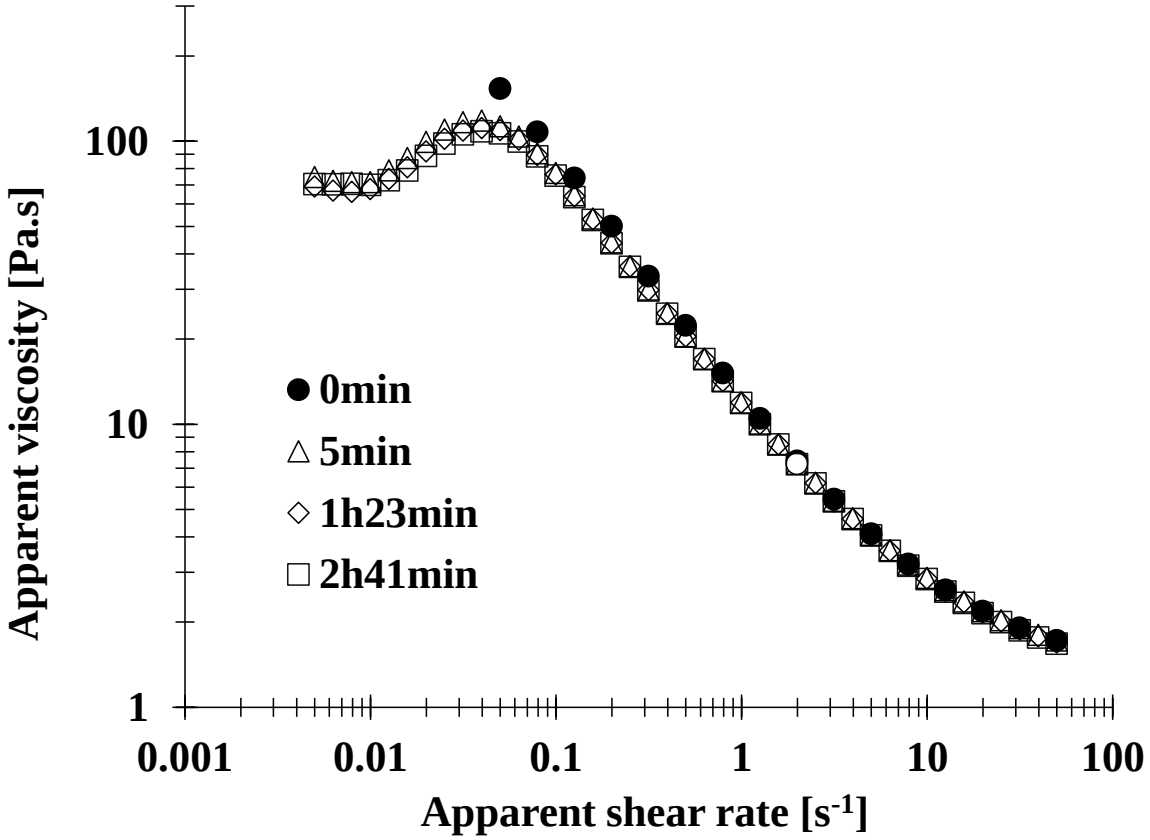

Fig.1: Apparent viscosity *vs* apparent shear rate evolutions at different times for the same molten chocolate sample measured with a 1mm gap smooth plate-plate. Solid dots (0min) represent the first increasing ramp. Open symbols: triangles (5min), diamonds (1h23min) and squares (2h41), represent decreasing ramps. The symbols show respectively steps number 1,2,6 and 10 of the proposed protocol.

Whatever the starting time of the measured decreasing ramp (5min, 1h23 or 2h41min), all apparent flow curves were shown to be perfectly superimposed, providing that a steady state was reached. Thus, each measured point was accepted as valid if the comparison of five consecutive recordings were within a tolerance limit of 2% within a time interval of 50 seconds maximum (cf Table 1b).

If the tolerance limit was over 2%, the last value measured (at 50s) was selected. In addition, measurements were made at minimum in triplicate giving a maximum experimental error of 11%. The middle ramp was only selected for further exploitation in the case of perfect replicate superimposition implying that the surrounding ramps have been used as references.

By assuming either sugar and cocoa particles to be spheres of diameter d_{part}≈20µm with a density of ~1500 kg/m^3 dispersed in a continuous fat cocoa butter phase at 40°C (ρ_{cont}=900 kg/m^3, μ_{cont}=100Pa.s), a quick estimate of the sedimentation velocity, assuming no inter-particle interactions, v_{sed} is given in the order of 5.10^{-8}m/s by :

$$v_{sed} = \frac{{d_{part}}^2(\rho_{part}-\rho_{cont})g}{18.\mu_{cont}} \qquad (1)$$

The corresponding sedimentation time h/v_{sed} inside the plate-plate geometry is therefore around 50 hours for a 1mm gap width. Knowing that an increasing-decreasing shear rates ramps cycle takes about 38 minutes, we can deduce that no sedimentation took place in our experiments. This is confirmed by the perfect superimposition of all the curves in Fig.1.

Finally, the normal force, *i.e.* perpendicular to the rotation plane, will not be displayed here as the entire measurement campaign values remained within the 15±10mN interval.

3. Results and discussion

1mm-gap raw flow curves of Fig.1 showed an apparent Newtonian plateau followed by an apparent shear-thickening and a shear-thinning behavior when increasing shear rate values. If the shear stress *vs* shear rates are represented (Fig.2), one can see distinct but slightly curved lines in the lower part of the

graph which change abruptly into a further much more accentuated curve. The pseudo Newtonian plateau and shear-thickening behavior in Fig.1 correspond to the lower part of the graph in Fig.2 while the shear-thinning behavior in Fig.1 is illustrated by the more accentuated curve in the second figure. At other gap values, similar behaviors were observed albeit with an abrupt change observed for the lower shear rate when increasing the gap size.

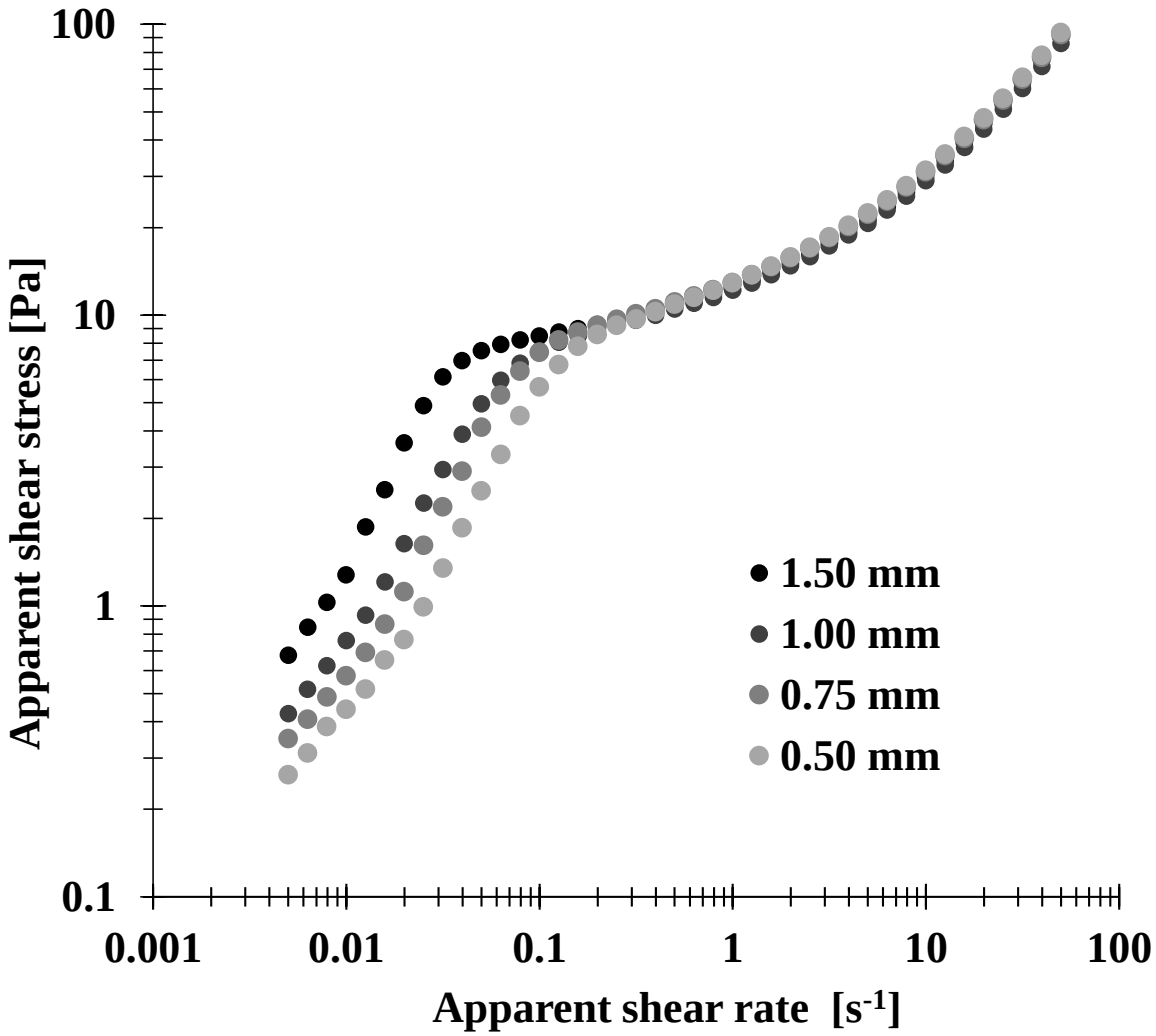

Fig.2: Examples of apparent shear stress *vs* shear rates curves obtained at 1.50mm, 1.00mm, 0.75mm and 0.50 mm gaps.

This shear stress *vs* apparent shear rates representation has strong similarities to other concentrated suspensions or complex yield stress fluids, for

instance, gels (Clasen, 2012; Meeker et al., 2004a, 2004b), mayonnaise (Clasen et al., 2006), fiber pulp suspensions (Derakhshandeh et al., 2010), toothpaste (Ardakani et al., 2011), shaving foam, emulsions (Bertola et al., 2003) or liquid foams (Laporte et al., 2015). This type of behavior, for which the measurements are well superimposed at high values, while remaining highly dependent on the characteristic gap length at low values is usually interpreted as the presence of a fluid wall slip (Bertola et al., 2003; Cloitre and Bonnecaze, 2017; El Kissi et al., 2006; Hatzikiriakos, 2015; Meeker et al., 2004a, 2004b; Poumaere et al., 2014; Sochi, 2011).

3.1. Corrections of rheometrical raw data

3.1.1. Shear stress correction

The science of rheology is based on the experimental determination of the material constitutive equation that links shear rate and shear stress, respectively imposed and measured by the rheometer. In the simplest shear flow configuration, the fluid is contained and sheared between two parallel circular plates in relative rotation, at a velocity Ω [rad.s^{-1}] around the vertical axis (Oz) and separated by a distance H (Fig.3a).

In plate-plate geometry, a homogeneous fluid shows a velocity field reduced to its tangential component $v_\theta(r,z)$ which depends solely on the distance of the rotational axis and of the vertical position in the gap z:

$$v_\theta(r,z) = \Omega.r.z/H \qquad (2)$$

The corresponding apparent local shear rate is expressed as:

$$\dot{\gamma}_a(r) = \frac{dv_\theta}{dz} = \frac{\Omega r}{H} \qquad (3)$$

Inside the gap, the shear stress $\tau(r)$ is related to the torque Γ as follows:

$$\Gamma = \int_0^R 2\pi r^2 \tau(r) dr \qquad (4)$$

Considering Eq.3, the torque may be rewritten as:

$$\Gamma = \frac{2\pi H^3}{\Omega^3} \int_0^{\dot{\gamma}_a(R)} \dot{\gamma}_a^2 \, \tau(\dot{\gamma}_a) d\dot{\gamma}_a \qquad (5)$$

and at the rim of plate-plate geometry, the differentiation of Eq.5 finally gives (Mooney, 1931; Rabinowitsch, 1929; Yilmazer and Kalyon, 1989):

$$\tau_R = \tau(\dot{\gamma}_a(R)) = \left(3 + \frac{dln\Gamma}{dln\dot{\gamma}_a(R)}\right) \frac{\Gamma}{2\pi R^3} \qquad (6)$$

In all these equations, the "*a*" and "*R*" indices are representative of the words "apparent" and "rim". In the case of Newtonian viscous fluid, the raw shear stress which may also be called apparent shear stress, is expressed as:

$$\tau_{app}(\dot{\gamma}_{a,R}) = \tau_{Newtonian}(\dot{\gamma}_{a,R}) = \frac{2\Gamma}{\pi R^3} \qquad (7)$$

At this stage, we can report that a similar correction on a Non-Newtonian aqueous hydroxyethyl cellulose solution directly carried on the viscosity was published by Krieger in 1966 (Krieger, 1966). This alternative yields corrected viscosity values obviously identical to those obtained *via* Eq.6.

(a) ***(b)***

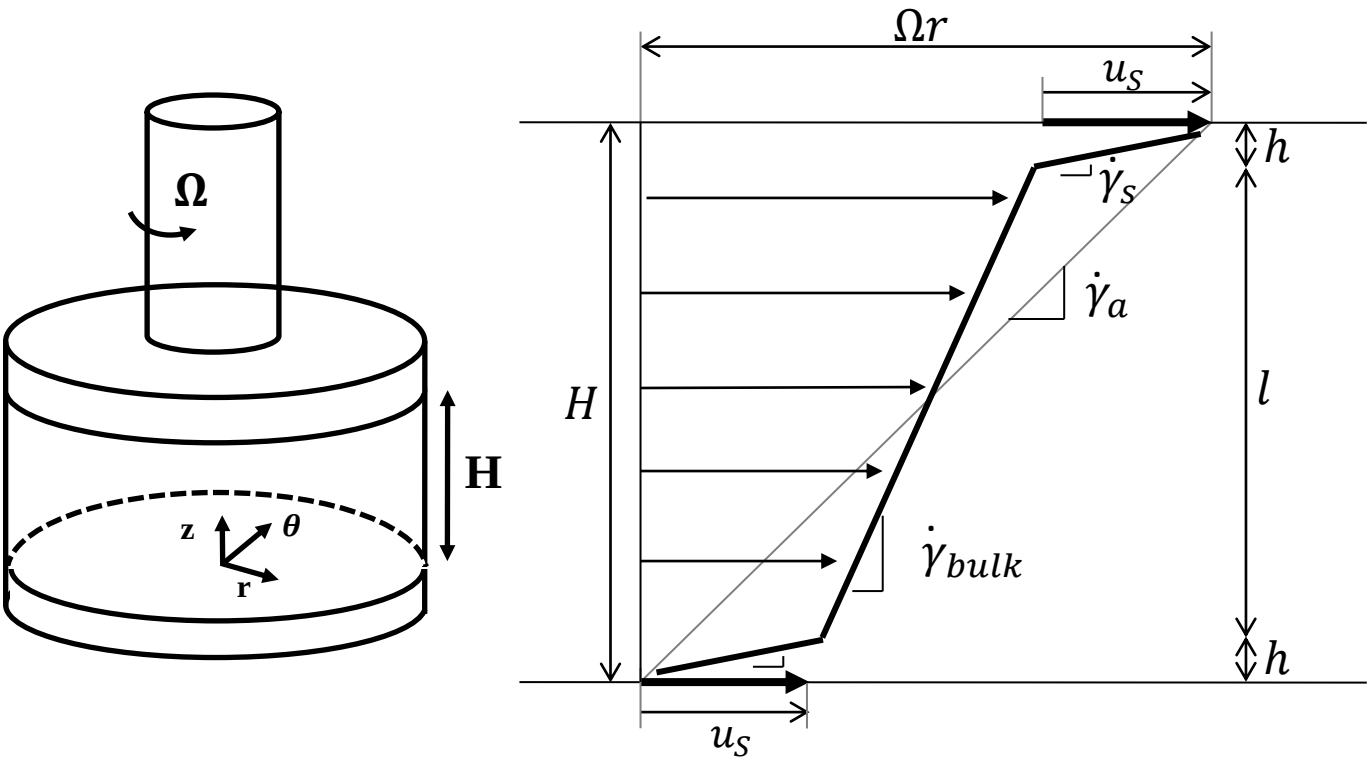

Fig.3: (a) Schematic drawing of parallel plate-plate geometry. (b) Focus on the velocity field inside the geometry gap in the presence of slip at the solid wall.

In Fig.4, two sets of selected data are represented symbolized by solid dots and solid lines. The solid dots represent the mean values of the triplicates of the raw (or apparent) data previously introduced in Fig.2.

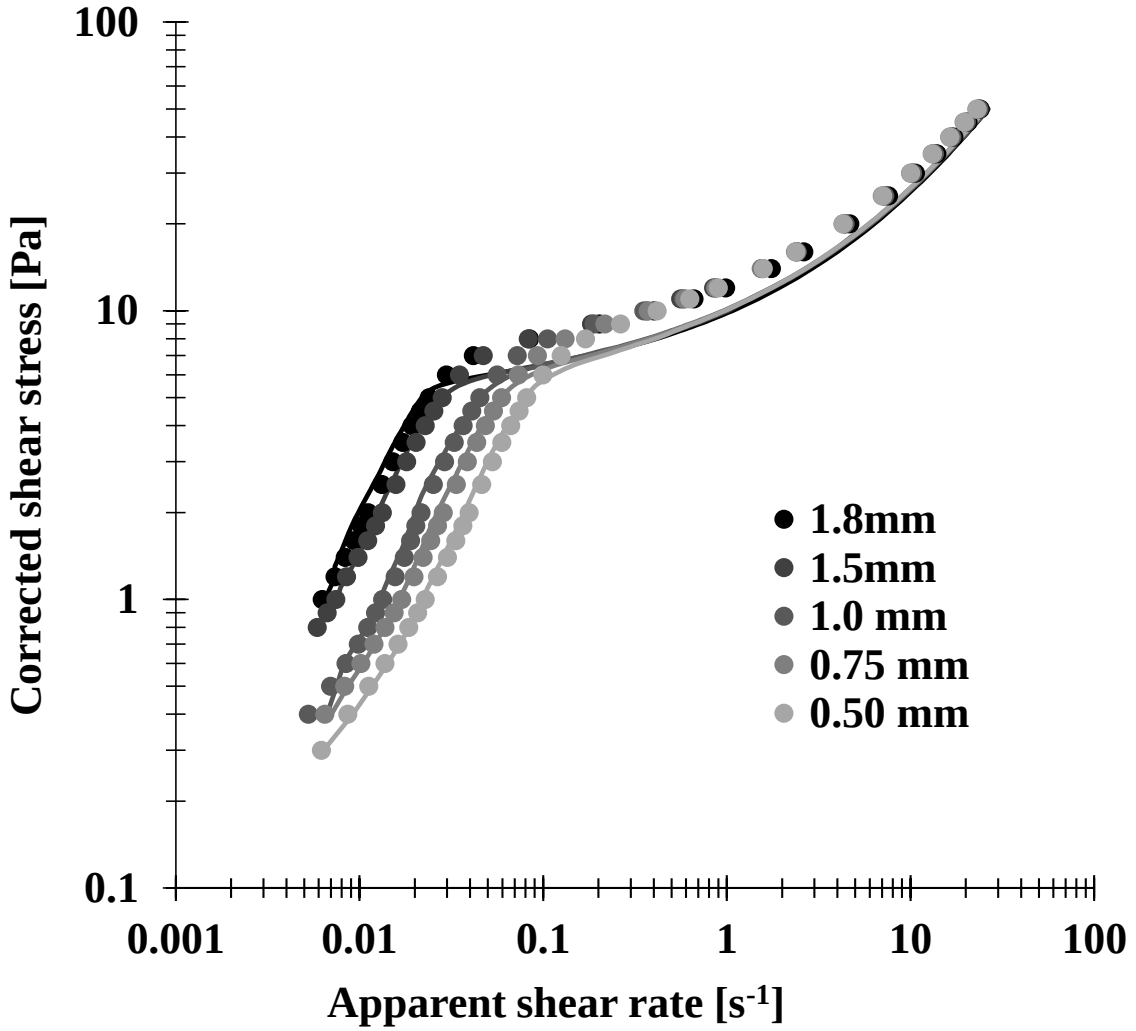

Fig.4: Corrected shear stress versus apparent shear rate curves. The solid symbols are the mean values of interpolated data. The solid lines are the mean values of both the corrected and interpolated data. All experiments were carried out with a smooth plate-plate geometry at varying gap size: 1.8mm, 1.5mm, 1mm, 0.75 mm and 0.5 mm.

The solid lines are the result of the shear stress correction calculated by using Eq.6. Cubic smoothing spline "csaps" interpolations (using Matlab software) were applied to the raw data in order to compute the triplicate mean values and allow further constant shear stress calculations. At high shear stresses (*i.e.* high shear rates) the raw data is seen above the corresponding solid lines, reflecting an overestimation without correction. Also, a more complete overlapping at high values after correction can be seen. Conversely, at low shear

stresses, the raw data is below the corresponding solid lines leading to an underestimation of the apparent shear stress without correction.

3.1.2. Shear rate correction

Once the shear stress had been corrected, attention was focused on the correction of the shear rate values. To do this, the sample inside the plate-plate tool illustrated in Fig.3 was used again as follows. With a motionless lower plate, the upper plate was rotated around the (Oz) axis at a rotation speed Ω. Where there was presence of slippage phenomena at the solid walls, *i.e.* at z=0 and z=H in Fig.3b, the apparent shear rate was no longer homogeneous. This wall slippage can be understood macroscopically as the effect of a thin depleted layer at the solid walls sandwiching the bulk material (Barnes, 1995; Cloitre and Bonnecaze, 2017; Meeker et al., 2004a, 2004a). This depleted layer of thickness h is submitted to a high shear rate near the solid walls whereas on the bulk length l the rest of the fluid remains less sheared.

Based on Mooney's pioneer work (Mooney, 1931), the apparent slip velocity $u_s(r)$ at the solid walls is expressed as:

$$\Omega r = \dot{\gamma}_{bulk}(r).\, l + 2.\dot{\gamma}_s(r).\, h = \dot{\gamma}_{bulk}(r).\, l + 2.u_s(r) \qquad (8)$$

where $\dot{\gamma}_{bulk}$ and $\dot{\gamma}_s$ are the shear rates in the bulk and in the depleted layer, respectively. A schematic drawing of the slip between the plates can be seen in Fig.3b.

Assuming $h \ll l$ and $h \ll H$, with $H = 2l + h$ is the total length between the two plates, the apparent shear rate at the rim $\dot{\gamma}_a(R)$, can be written as:

$$\dot{\gamma}_a(R) = \frac{\Omega R}{H} = \dot{\gamma}_{bulk}(R) + \frac{2u_s(R)}{H} \qquad (9)$$

Using the fact that the constitutive equation links the shear stress and the shear rate, Eq.9 can also be written as:

$$\dot{\gamma}_a(\tau_R) = \frac{\Omega R}{H} = \dot{\gamma}_{bulk}(\tau_R) + \frac{2u_s(\tau_R)}{H} \quad (10)$$

where $\dot{\gamma}_{bulk}(\tau_R)$ is the bulk shear rate at a given wall stress value, τ_R, and $u_s(\tau_R)$ is the wall slip velocity at the same shear stress. In Eq.10, the bulk shear rate and the slip velocity are expressed at a fixed shear stress τ_R. In the rheological trials conducted here, all measurements were handled at fixed shear rates. As previously mentioned (§ 3.1.1), all shear stress data was corrected and interpolated with a "csaps" tool in order to use Eq.10 at a fixed shear stress τ_R.

Fig.5a-c details the apparent shear rate *vs* the reciprocal gap at different shear stresses in order to compare experimental data in the model expressed by Eq.10. Fig.6 gives a summary of the different behaviors detailed below.

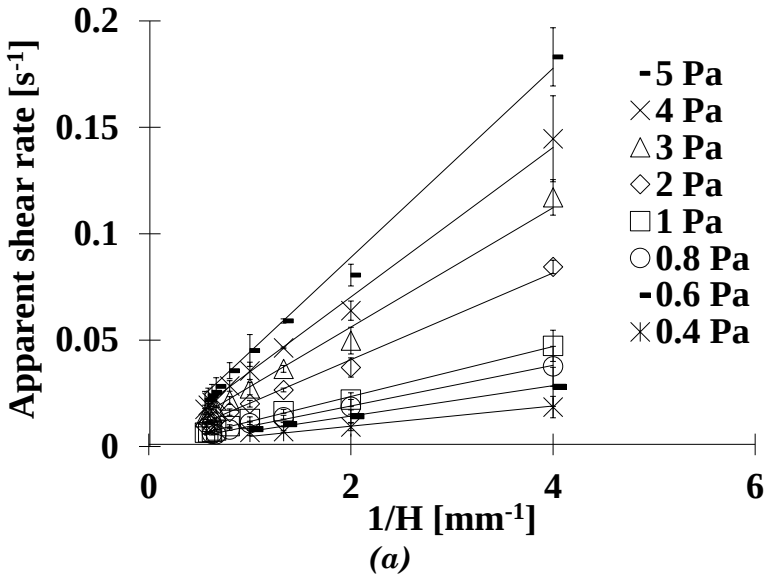

(a)

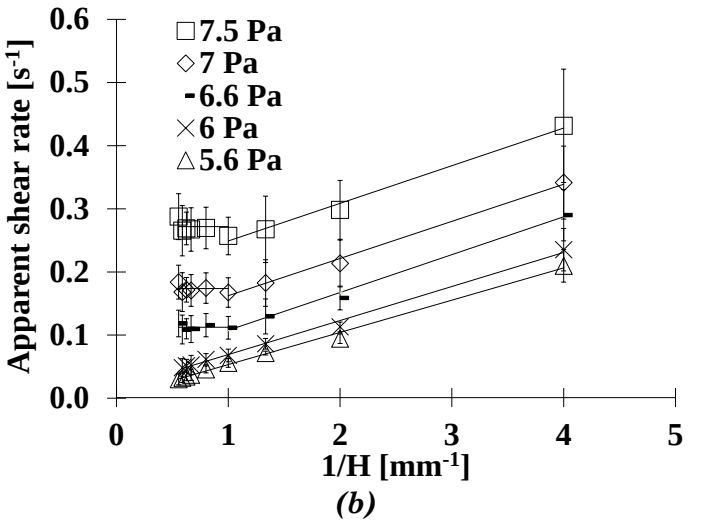

(b)

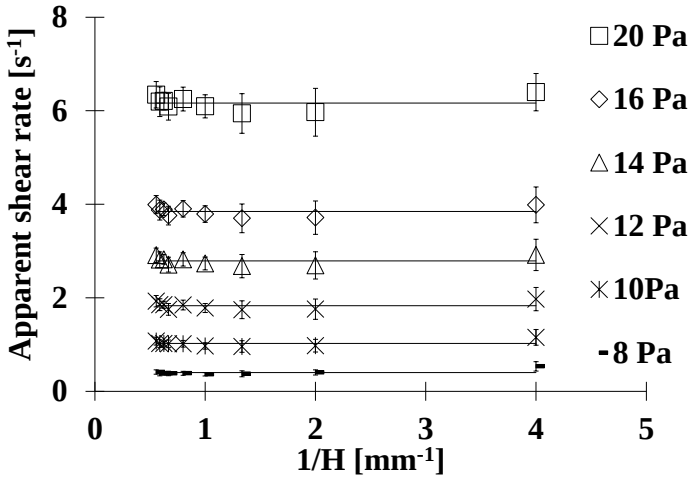

(c)

Fig.5: Apparent shear rate as a function of the reciprocal gap for different constant shear stresses. Details of each encountered behavior: (a) low shear rate: pure slip regime, (b) intermediate shear rate: transition regime (c) high shear rate: homogeneous bulk shear regime.

This representation of the apparent shear rate *vs* 1/H has been used for highly filled suspensions in the past (Yilmazer and Kalyon, 1989). As illustrated by Figs.5a, 5b and 5c, our data has been split into three different plots.

In Fig.5a for low shear stresses, the apparent shear rates are shown to be strictly proportional to 1/H. According to Eq.10, the best fit of experimental data is reduced to an affine function where only wall slip occurs (Fig.6, green region). The apparent shear of the sample is then reduced to a solid-like slippage at the wall, whereas the "fluid" bulk remains unsheared but only elastically distorted.

In Fig.5c for high shear stresses, apparent shear rates are represented by the horizontal straight lines (Fig.6, blue region). Thus, in Eq.10 the bulk shear rate $\dot{\gamma}_{bulk}(\tau_R)$ contribution largely exceeds the terms of slippage $\frac{2u_s(\tau_R)}{H}$ implying equality between applied and measured shear rates.

In Fig.5b for intermediate shear stresses, the apparent shear rates are no longer proportional to 1/H but, rather, composed of two straight lines joined at 1/H=1.33 mm^{-1} (or 0.75 mm equivalent gap), therefore implying two ranges for the use of Eq.10. At 1/H values below 1.33mm^{-1} (blue region, Fig.6) the chocolate behaves as a liquid-like material without any slip velocity. This behavior is identical to that of Fig.5c where the slip velocity term in Eq.10 is negligible. Above 1.33 mm^{-1} (red region), the chocolate may take on a partially liquid and also a partially solid form so both the two terms of Eq.10 must be considered when data are adjusted. For instance, at 6.6 Pa, the fit of experimental data gives the slip velocity u_s equal to 0.03m/s and a bulk shear rate $\dot{\gamma}_{bulk}$ of 0.05s^{-1}. The reciprocal length 1/H=1.33mm^{-1} is consequently the separating line between these two different behaviors or regimes and is surely a consequence of confinement of the particles which measure approximately 20 µm. This same transition 1/H=1.33 mm^{-1} corresponds to H=750 µm, indicating that the gap is only ~40 times the size of an average particle and therefore relatively small. This value seems to be the limit for distinguishing between an “equivalent granular” or alternatively a continuous view of the molten chocolate used here. The “equivalent granular” material flows more like a solid while the continuous material will flows more like a liquid (Liu and Nagel, 1998). Without going further in the interpretation of such behavior, it can be argued that the transition

313 driven by the 1/H value, *i.e.* by the gap size, is due to a localized *"cooperative flow*
314 *event*". Such an event affects the fluidity which is highly dependent on the ratio of
315 H to particle size (Coussot, 2014; Goyon et al., 2010).

316 A second important parameter that drives chocolate flow or not is the
317 experiment duration. For experiments of short duration, the material will be
318 elastically distorted but will not flow. For experiments which are longer, the
319 material will first be distorted and then, depending on the stress applied, will
320 flow after either a short or a substantially longer time as shown in the existing
321 literature (Auffret et al., 2009; Benmouffok-Benbelkacem et al., 2010; Caton and
322 Baravian, 2008; Cheddadi et al., 2012; Coussot, 2014; Ovarlez, 2011; Ovarlez and
323 Chateau, 2008; Saramito, 2007).

324 To conclude this section, Fig.6 summarizes what must be borne in mind
325 and what interpretation is to be given to the symbols on the right. For low shear
326 stresses (in green), the flow chocolate behaves as a solid-like slippage at the wall
327 (insert (a), Fig.6). For high or intermediate shear stresses and small 1/H (in blue),
328 the chocolate behaves as a liquid-like material without any slip velocity at the
329 walls (insert (c), Fig.6). For intermediate shear stresses (in red), the chocolate
330 behaves partially as liquid and also partially as solid material showing
331 simultaneously the behaviors of both bulk flow and slip at the walls (insert (b),
332 Fig.6). This latter case is interpreted to be a consequence of the non-homogeneous
333 shear rate distribution within the gap induced by the progressive fluidization of
334 the yield stress fluid.

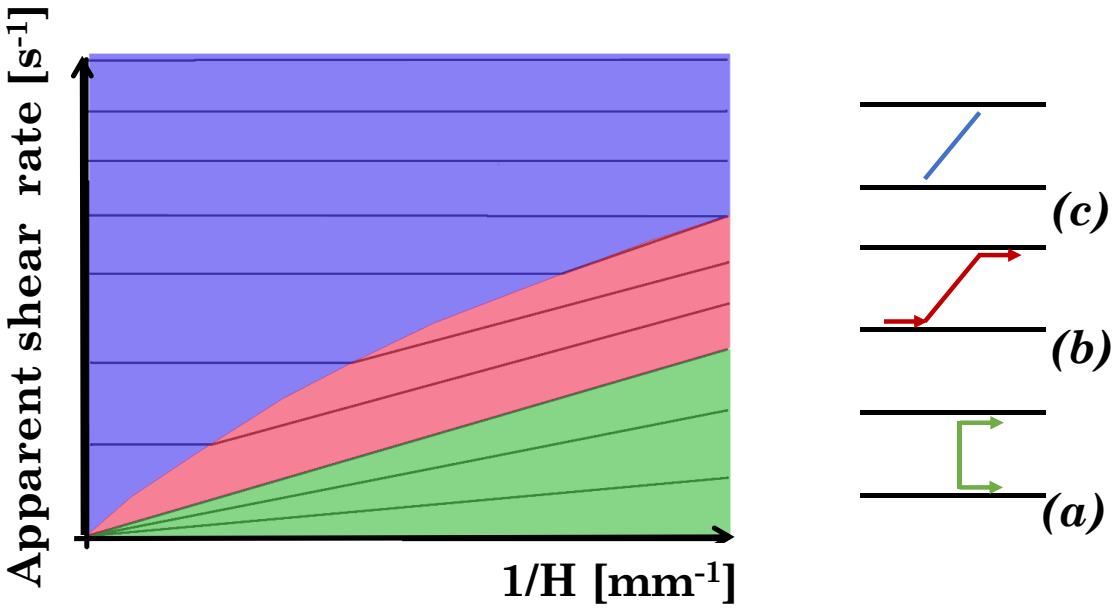

335

336 **Fig.6:** Apparent shear rate as a function of the reciprocal gap for different constant
337 shear stresses represented by the solid lines. A summary of the different behaviors
338 encountered on the left is symbolized by the three representations on the right: (a) at low
339 shear rate (in green), a pure slip regime, (b) at intermediate shear rate (in red), a
340 transition regime (c) at high shear rate (in blue), a homogeneous bulk shear regime.
341

342 As a consequence, a compromise has to be found between the required level
343 of characterization and the corresponding period available to carry out the
344 assays. In fact, the cost necessary to accurately determine the yield stress value
345 will be proportional to the measurement duration. From an industrial point of
346 view, applying the present method to a few well selected gap values, *e.g.* two or
347 three, may be sufficient, particularly if a well-defined programming procedure is
348 used. By contrast, to distinguish between products possessing very similar
349 behaviors, *e.g.* two molten chocolates of similar composition and particle size, a
350 longer duration and a greater number of experiments will be required.

351 From a scientific point of view, the generalization of this method could help
352 to provide some clues to a deeper understanding of flow types close to the yield

353 stress. In addition, the tool presented here can also be used in numerical studies
354 to set the boundary conditions at solid walls.

355 *3.1.3. Conventional Yoshimura and Prudhomme correction*

356 Based on the continuum hypothesis of shear stress within the gap (cf 3.1.1), the
357 conventional *Yoshimura and Prudhomme* method (Yoshimura and Prud'homme,
358 1988) proposed the use of two series of experimental data carried out at H_1 and
359 H_2 gap sizes, which allows the calculation of the apparent shear rate and
360 viscosity at a given shear stress :

361 $$\dot{\gamma}_{aR}(\tau_R) = \frac{H_1\dot{\gamma}_{aR1}(\tau_R) - H_2\dot{\gamma}_{aR2}(\tau_R)}{H_1 - H_2} \quad (11)$$

362 $$\eta(\dot{\gamma}_{aR}) = \frac{\tau_R(H_1 - H_2)}{H_1\dot{\gamma}_{aR1}(\tau_R) - H_2\dot{\gamma}_{aR2}(\tau_R)} \quad (12)$$

363 Slip velocity may also be directly deduced:

364 $$u_{s,Y\&P}(\tau_R) = \frac{\dot{\gamma}_{aR1}(\tau_R) - \dot{\gamma}_{aR2}(\tau_R)}{2\left(\frac{1}{H_1} - \frac{1}{H_2}\right)} \quad (13)$$

365 Hereinafter, we will apply these formula to the interpolated and shear stress
366 corrected data in §3.1.1.

367 ***3.2. Wall slip velocity***

368 In Fig.7, the solid triangles represent the wall slip velocity $u_s(mm/s)$ in
369 relation to the shear stress τ_R (Pa). The wall slip velocity was obtained from the
370 data represented in Fig.5a to 5c and by using Eq.10. Below 5.4Pa in the green
371 region, the slip velocity u_s follows an affine function of slope u_s/τ_R =4.55×10^{-3}
372 ±4.11×10^{-5} mm/(Pa.s). For these stresses, the chocolate behaves as a solid-like
373 material. Above 8Pa in the blue region, the slip velocity symbolized by the thick
374 solid line at the bottom is negligible. In this domain, the chocolate is fully
375 sheared without any slip velocity at the walls.

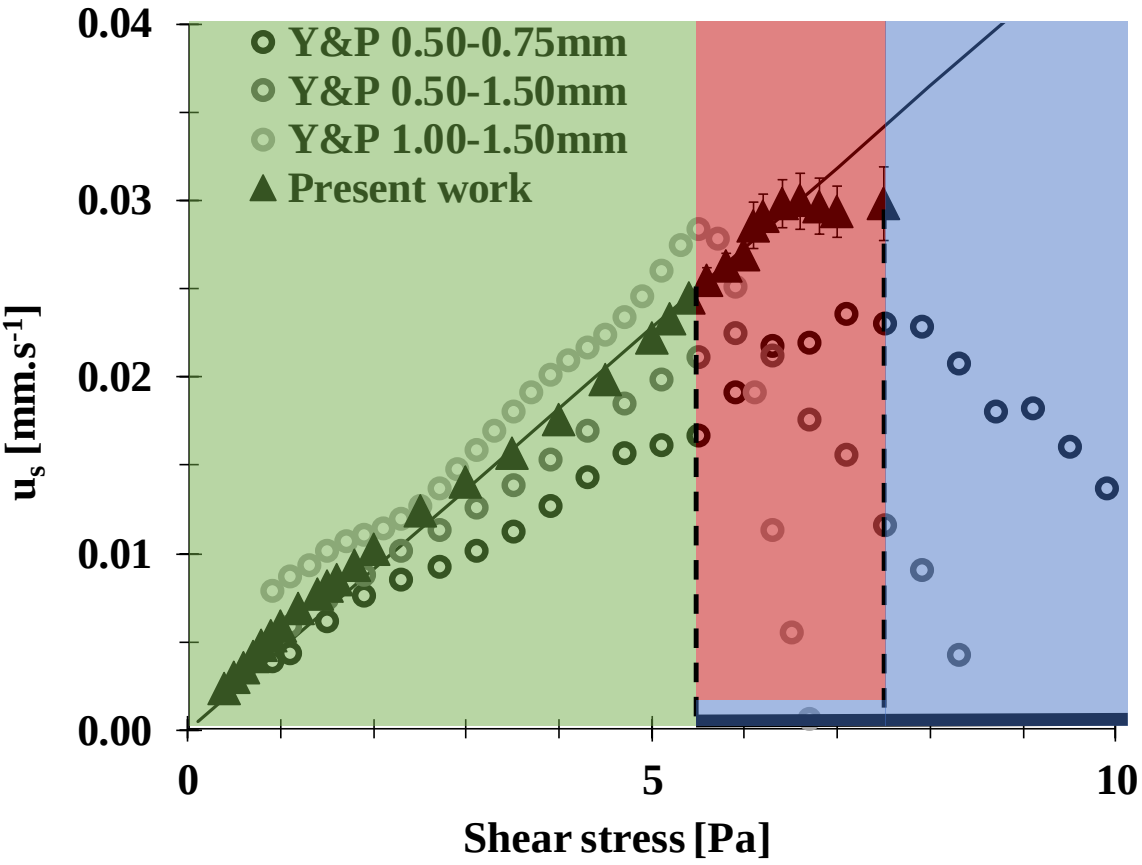

Fig.7: Wall slip velocity as a function of the shear stress. The solid triangle symbols illustrate experimental data from the present work. The solid line represents the correspondingly best linear fit ($u_s = 4.55.10^{-3}\tau_R$). The open circle symbols represent the wall slip velocity evolution obtained using the *Yoshimura and Prud'homme* method with 0.50-0.75 mm; 0.50-1.50 and 1.00-1.50 mm gaps pair.

Between 5.4Pa and 8Pa, two slip velocities are obtained. For a constant shear stress at low 1/H values, there is no slip velocity as represented by the horizontal lines in Fig.5b. These results are represented by the thick solid line in the blue region in Fig.7. At high 1/H values, the fit of the linear shapes in Fig.5b using the Eq.10, as previously explained, returns not only values of an effective shear rate but also a constant slip velocity u_s of approximately 0.03mm/s whatever the applied stress, as represented by the triangles in the red region in Fig.7.

391 In the existing literature, slip velocity is assumed to be either proportional
392 (Russel and Grant, 2000) or quadratically dependent on the shear stress (Clasen,
393 2012; Meeker et al., 2004b; Salmon et al., 2003; Yeow et al., 2006). However, at
394 this stage there is no obvious explanation for these differences.

395 A path worthy of consideration could be seen in Fig.7 by open circle
396 symbols representing data obtained using the *Yoshimura and Prud'homme*
397 method (Yoshimura and Prud'homme, 1988) applied at 0.50-0.75 mm; 0.50-1.50
398 and 1.00-1.50 mm gaps pair, respectively. Clearly, the *Yoshimura and*
399 *Prud'homme* method produces different results in relation to the gaps pair used.
400 Furthermore, the velocity curves show surprising concave shapes characterized
401 by a maximum occurring in the intermediate shear stress region (red region). At
402 low stresses (green region), the difficulty in reproducing the same slip velocity
403 evaluation when the gaps pair is changed can be interpreted as the result of a
404 combination of experimental errors and of the difference between the two gaps.
405 At intermediate stresses (red region), the decrease in the slip velocity is induced
406 by the use of Eq.13 at two reciprocal gaps $1/H_1$ and $1/H_2$, within two different
407 regions, for instance, the red region for $1/H_1$ and the blue region for $1/H_2$ in Fig.6.
408 In this case, it becomes obvious that the necessity of following a constant shear
409 stress line to join a shear rate couple, at $1/H_1$ and $1/H_2$ values respectively, will
410 not be satisfied.

411 For these reasons, we do not recommend the use of the *Yoshimura and*
412 *Prud'homme* method on all yield stress fluids in order to determine the slip *vs*
413 stress evolution and even less so for conditions close to the yield stress.

414 ***3.3. Reconstitution of the steady state bulk flow curve***

The effective viscosity *vs* the bulk shear rate figure can now be reconstituted (Fig.8). The effective viscosity is computed by a simple division of the corrected shear stress (§3.1.1) by the effective (or bulk) shear rate (§3.1.2). In contrast to Fig.1 the present work led to a yield stress fluid behavior depicted by a continuous decrease of the effective viscosity *vs* the bulk shear rate. The apparent Newtonian plateau followed by an apparent shear-thickening behavior in Fig.1 completely disappeared when the corrections proposed in this article were applied. Nonetheless, this is not the case for our data (open circles, Fig.8) to which we applied the *Yoshimura and Prud'homme* correction. Indeed, this last figure shows a Newtonian plateau for the different selected gaps pair. Moreover, the plateau value will depend on the selected gaps pair.

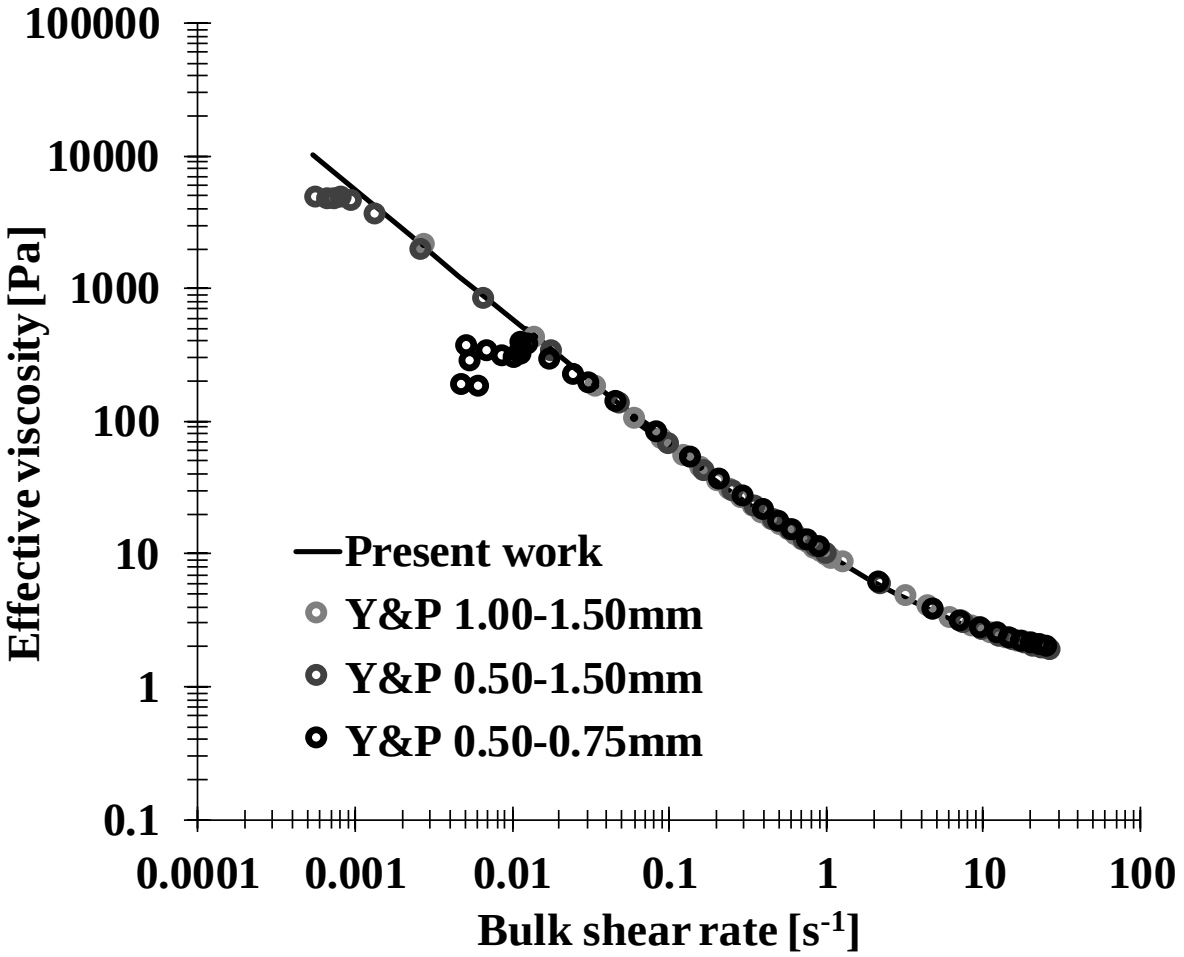

427

428 **Fig.8:** Evolution of the effective viscosity *vs* bulk shear rate. The solid line represents the
429 present work's corrected data. Open circles represent the data obtained *via* the
430 *Yoshimura and Prud'homme* method with 1.00-1.50mm; 0.50-1.50 and 0.50-0.75mm gaps
431 pair.
432
433 Finally, Fig.9 shows the evolution of the corrected shear stresses (§3.1.1) *vs*
434 bulk shear rates (§3.1.2) evolutions in logarithmic scales. This representation is
435 one of the most common representations of yield stress fluid.

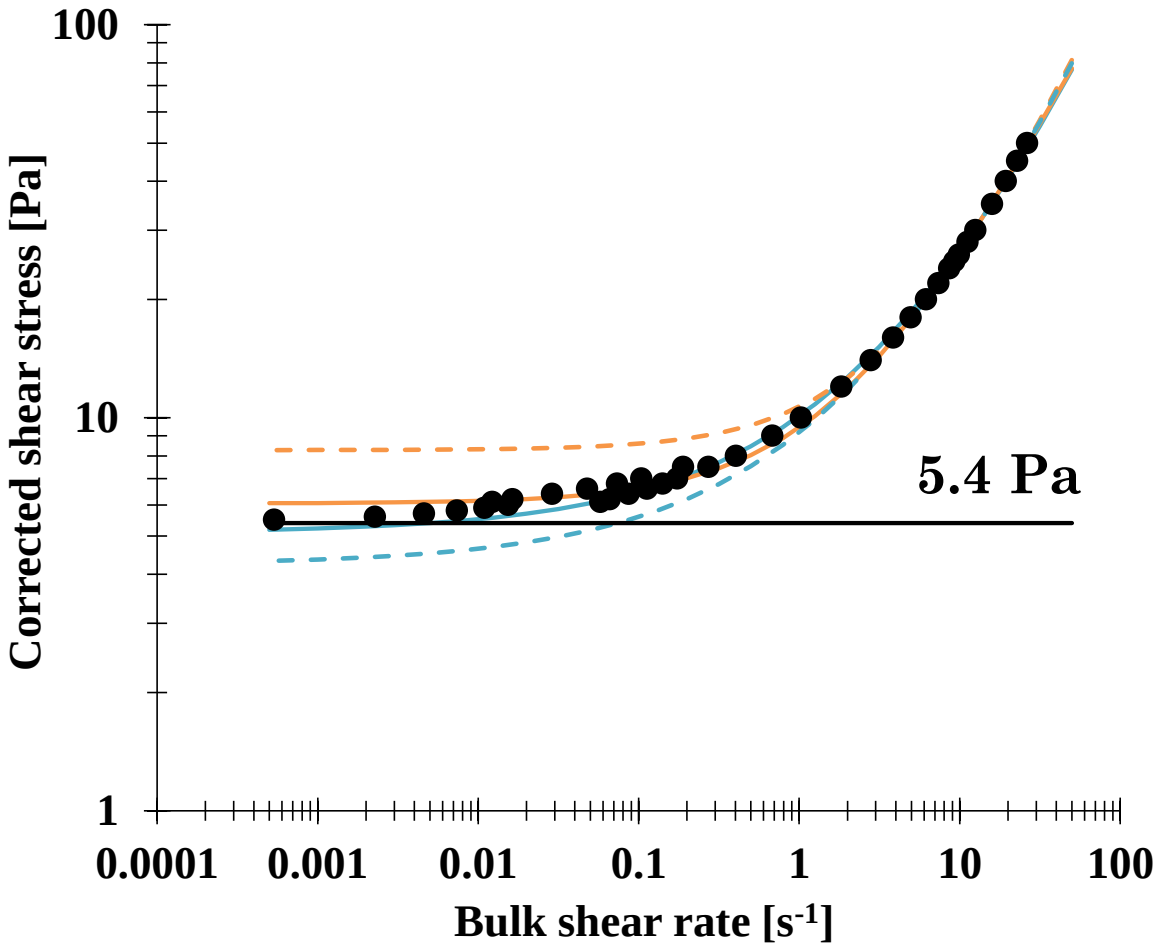

Fig.9: Evolution of corrected shear stress *vs* bulk shear rate (solid circle symbols). The lines correspond to the different data fittings using *Casson* (in blue) and *Herschel-bulkley* (in orange) as models. Broken lines refer to the IOCCC standard conditions, *i.e.* a $2s^{-1}$-$50s^{-1}$ fitting while solid lines refer to a fit over the entire range of data, *i.e.* a 0.005-$50s^{-1}$ fitting.

Below a critical stress, also called bulk yield stress, of 5.4 Pa the shear rate is zero and no flow occurs. Up to 5.4Pa, the shear rate is not equal to zero and so the fluid flows, apparently with a linear stress to shear rate dependence. As the log-log scale representation expands low values, this representation is particularly suitable for focusing on the surrounding yield stress where values tend to be constant.

Additional solid lines in Fig.9 represent the fits using conventional *Casson* and *Herschel-Bulkley* models on the shear rate range of IOCCC recommendations from 2 to $50s^{-1}$ (broken lines) but also on the entire range of data, from 0.005 to

452 $50s^{-1}$ (solid lines). As a reminder, the *Herschel-Bulkley* (Eq.14) and *Casson*
453 (Eq.15) constitutive equations are expressed as:

454 $$\sigma = \sigma_{0,HB} + k_{HB}\dot{\gamma}^n \quad (14)$$

455 $$\sqrt{\sigma} = \sqrt{\sigma_{O,C}} + \sqrt{\eta_C \dot{\gamma}} \quad (15)$$

456 where $\sigma_{0,HB}$, k_{HB}, n are respectively the *Herschel-Bulkley* yield stress, the
457 consistency index and the flow index parameters, on the one hand, and $\sigma_{0,C}$, η_C
458 are respectively the *Casson* yield stress and the viscosity on the other hand.
459 Table 2 summarizes all obtained parameters from the fitting of corrected data
460 from the IOCCC standard conditions ($2\text{-}50s^{-1}$) and also for the extended
461 conditions ($0.005\text{-}50s^{-1}$) with Eq.14 and Eq15.

462 ***Table 2:*** *Summary of the different parameters obtained by fitting the molten chocolate*
463 *data with the Herschel-Bulkley and Casson models. The symbol * indicates deviation*
464 *from the bulk yield stress 5.4Pa determined directly in Fig.5.*
465

Shear rate range for fittings	Corrected data	
	Herschel-Bulkley	Casson
	$\sigma = \sigma_{0,HB} + k_{HB}\dot{\gamma}^n$	$\sqrt{\sigma} = \sqrt{\sigma_C} + \sqrt{\eta_C \dot{\gamma}}$
Standard conditions ($2\text{-}50s^{-1}$)	$\sigma_{0,HB}$=8.27±0.14Pa (1.7 %) (53%)* k_{HB}=2.38±0.06Pa.s^n (2.3%) n_{HB}=0.876±0.006 (0.7%)	$\sigma_{0,c}$=4.23±0.10 Pa (2.3%) (22%)* η_c=0.94±0.01 Pa.s (1.3%)
Extended conditions ($0.005\text{-}50s^{-1}$)	$\sigma_{0,HB}$ =6.05 ±0.08Pa (1.3%) (12%)* k_{HB}=3.39±0.08Pa.s^n (2.4%) n_{HB}=0.780±0.008 (1.0%)	$\sigma_{0,c}$ =5.10±0.08 Pa (1.7%) (5.6%)* η_c=0.85±0.01 Pa.s (1.3%)

466

467 From Fig.9 and Table 2, it can be observed that the *Herschel-Bulkley* model is
468 systematically above experimental data whereas the *Casson* model is
469 systematically below them. Moreover, both models applied within the range of
470 the IOCCC standard recommendation reveal a larger discrepancy. Indeed, as an
471 example, the *Herschel-Bulkley* model gives a yield stress of 8.27±0.14Pa rather
472 than the 5.4±0.2Pa directly determined in Fig.5. It is slightly better for the
473 *Casson* model which gives a yield stress of 4.23±0.10 Pa.

For both models, the viscosity, consistency and pseudo plastic index are summarized in Table 2 in addition to the yield stress value. All these estimations constitute useful data to characterize a yield stress fluid properly.

It should be noted that the evaluation of the yield stress by using both the *Casson* and *Herschel-Bulkley* models is of particular interest in the present case, as these models respectively under and overestimate it. This point could be a subject worthy of further study. Finally, we can also notice that the first stress value for which the molten chocolate begins to flow in Fig.5b (§3.1.2), represented by the horizontal line in Fig.9 at 5.4Pa, is in agreement with the yield stress obtained by using the best fits.

4. Conclusion

In this article we have proposed a simple and reliable method particularly well-adapted for the characterization of food materials showing yield stress behavior. This method allows identification of the constitutive and slip velocity law, and consequently an accurate evaluation of rheological parameters, essential for material characterization such as viscosity, consistency, pseudo plastic index, or yield stress. The level of accuracy of such parameters increases if, and only if, (i) an extended range of reciprocal gap is used and (ii) if all collected data are in an apparently steady state. This last condition can take a long time to obtain close to the yield stress.

The originality of this method lies in its capacity to take into account the correction of the slip velocity simultaneously with the non-homogeneity of the

flow field within the geometry gap. It also highlights the fact that the *Yoshimura and Prud'homme* method is inappropriate for yield stress fluid characterization.

Molten chocolate, given here as an example of an industrial multiphase product, was found to be a relatively simple material as it is not subject to aging, retarded viscoelasticity, thixotropy or sedimentation phenomena within the measurement duration. Nevertheless, the validity of our method remains to be demonstrated for more complex yield stress soft materials. Indeed, we can consider this method as applicable to model fluids as well as to more complex soft condensed shear thinning or viscoplastic materials or to industrial foodstuffs, which are not too heterogeneous at the scale of gap of the geometry. Provided, that a sufficient level of accuracy is reached, one can expect to be able to distinguish molten chocolates of similar formulations or other liquid foodstuffs.

Acknowledgments

The Laboratoire Rhéologie et Procédés is part of the LabEx Tec 21 (Investissements d'Avenir – grant agreement n°ANR-11-LABX-0030) and of the PolyNat Carnot Institut (Investissements d'Avenir – grant agreement n°ANR-11-CARN-030-01). Authors would like to gratefully acknowledge Susan Sinclair for proofing the manuscript.

References

520 Aeschlimann, J.-M., Beckett, S.T., 2000. International inter-laboratory trials to
521 determine the factors affecting the measurement of chocolate viscosity. J.
522 Texture Stud. 31, 541–576.
523 Afoakwa, E.O., Paterson, A., Fowler, M., 2008. Effects of particle size distribution
524 and composition on rheological properties of dark chocolate. Eur. Food
525 Res. Technol. 226, 1259–1268. https://doi.org/10.1007/s00217-007-0652-6
526 Afoakwa, E.O., Paterson, A., Fowler, M., Vieira, J., 2009. Comparison of
527 rheological models for determining dark chocolate viscosity. Int. J. Food
528 Sci. Technol. 44, 162–167. https://doi.org/10.1111/j.1365-2621.2008.01710.x
529 Ardakani, H.A., Mitsoulis, E., Hatzikiriakos, S.G., 2011. Thixotropic flow of
530 toothpaste through extrusion dies. J. Non-Newton. Fluid Mech. 166, 1262–
531 1271. https://doi.org/10.1016/j.jnnfm.2011.08.004
532 Auffret, Y., Roux, D.C.D., El Kissi, N., Dunstan, D.E., Pignot-Paintrand, I., 2009.
533 Stress and strain controlled rheometry on a concentrated lyotropic
534 lamellar phase of AOT/Water/Iso-octane. Rheol. Acta 48, 423–432.
535 https://doi.org/10.1007/s00397-008-0336-6
536 Balmforth, N.J., Frigaard, I.A., Ovarlez, G., 2014. Yielding to Stress: Recent
537 Developments in Viscoplastic Fluid Mechanics. Annu. Rev. Fluid Mech. 46,
538 121–146. https://doi.org/10.1146/annurev-fluid-010313-141424
539 Barnes, H.A., 1995. A review of the slip (wall depletion) of polymer solutions,
540 emulsions and particle suspensions in viscometers: its cause, character,
541 and cure. J. Non-Newton. Fluid Mech. 56, 221–251.
542 https://doi.org/10.1016/0377-0257(94)01282-M
543 Beckett, S.T., 2000. The science of chocolate. Royal Society of Chemistry.

544 Benmouffok-Benbelkacem, G., Caton, F., Baravian, C., Skali-Lami, S., 2010. Non-
545 linear viscoelasticity and temporal behavior of typical yield stress fluids:
546 Carbopol, Xanthan and Ketchup. Rheol. Acta 49, 305–314.
547 https://doi.org/10.1007/s00397-010-0430-4
548 Bertola, V., Bertrand, F., Tabuteau, H., Bonn, D., Coussot, P., 2003. Wall slip and
549 yielding in pasty materials. J. Rheol. 47, 1211–1226.
550 https://doi.org/10.1122/1.1595098
551 Bonn, D., Denn, M.M., 2009. Yield stress fluids slowly yield to analysis. Science
552 324, 1401–1402.
553 Bonn, D., Paredes, J., Denn, M.M., Berthier, L., Divoux, T., Manneville, S., 2015.
554 Yield Stress Materials in Soft Condensed Matter. ArXiv150205281 Cond-
555 Mat.
556 Caton, F., Baravian, C., 2008. Plastic behavior of some yield stress fluids: from
557 creep to long-time yield. Rheol. Acta 47, 601–607.
558 https://doi.org/10.1007/s00397-008-0267-2
559 Cheddadi, I., Saramito, P., Graner, F., 2012. Steady Couette flows of
560 elastoviscoplastic fluids are nonunique. J. Rheol. 56, 213–239.
561 https://doi.org/10.1122/1.3675605
562 Clasen, C., 2012. Determining the true slip of a yield stress material with a
563 sliding plate rheometer. Rheol. Acta 51, 883–890.
564 Clasen, C., Gearing, B.P., McKinley, G.H., 2006. The flexure-based microgap
565 rheometer (FMR). J. Rheol. 50, 883–905. https://doi.org/10.1122/1.2357190
566 Cloitre, M., Bonnecaze, R.T., 2017. A review on wall slip in high solid dispersions.
567 Rheol. Acta 56, 283–305. https://doi.org/10.1007/s00397-017-1002-7

568 Coussot, P., 2014. Yield stress fluid flows: A review of experimental data. J. Non-
569 Newton. Fluid Mech. 211, 31–49.
570 https://doi.org/10.1016/j.jnnfm.2014.05.006
571 Damianou, Y., Philippou, M., Kaoullas, G., Georgiou, G.C., 2014. Cessation of
572 viscoplastic Poiseuille flow with wall slip. J. Non-Newton. Fluid Mech. 203,
573 24–37.
574 Derakhshandeh, B., Hatzikiriakos, S.G., Bennington, C.P.J., 2010. Rheology of
575 pulp suspensions using ultrasonic Doppler velocimetry. Rheol. Acta 49,
576 1127–1140. https://doi.org/10.1007/s00397-010-0485-2
577 Divoux, T., Barentin, C., Manneville, S., 2011. From stress-induced fluidization
578 processes to Herschel-Bulkley behaviour in simple yield stress fluids. Soft
579 Matter 7, 8409–8418.
580 El Kissi, N., Nigen, S., Pignon, F., 2006. Glissement et Rhéométrie. Rhéologie 13–
581 39.
582 Goyon, J., Colin, A., Bocquet, L., 2010. How does a soft glassy material flow:
583 finite size effects, non local rheology , and flow cooperativity. Soft Matter 6,
584 2668–2678. https://doi.org/10.1039/C001930E
585 Grenard, V., Divoux, T., Taberlet, N., Manneville, S., 2014. Timescales in creep
586 and yielding of attractive gels. Soft Matter 10, 1555–1571.
587 Hatzikiriakos, S.G., 2015. Slip mechanisms in complex fluid flows. Soft Matter
588 11, 7851–7856.
589 Herzhaft, B., 2002. Correlation between transient shear experiments and
590 structure evolution of aqueous foams. J. Colloid Interface Sci. 247, 412–
591 423.

592 Herzhaft, B., Kakadjian, S., Moan, M., 2005. Measurement and modeling of the
593 flow behavior of aqueous foams using a recirculating pipe rheometer.
594 Colloids Surf. Physicochem. Eng. Asp., A collection of papers presented at
595 the 5th European Conference on Foams, Emulsions, and Applications,
596 EUFOAM 2004, University of Marne-la-Vallee, Champs sur Marne
597 (France), 5-8 July, 2004 263, 153–164.
598 https://doi.org/10.1016/j.colsurfa.2005.01.012
599 Krieger, I.M., 1966. Direct Determination of the Flow Curves of Non-Newtonian
600 Fluids. IV. Parallel-Plane Rotational Viscometer. J. Appl. Phys. 37, 4703.
601 https://doi.org/10.1063/1.1708121
602 Laporte, M., Della Valle, D., Loisel, C., Marze, S., Riaublanc, A., Montillet, A.,
603 2015. Rheological properties of food foams produced by SMX static mixers.
604 Food Hydrocoll. 43, 51–57. https://doi.org/10.1016/j.foodhyd.2014.04.035
605 Lidon, P., Villa, L., Manneville, S., 2017. Power-law creep and residual stresses
606 in a carbopol gel. Rheol. Acta 56, 307–323. https://doi.org/10.1007/s00397-
607 016-0961-4
608 Liu, A.J., Nagel, S.R., 1998. Nonlinear dynamics: Jamming is not just cool any
609 more. Nature 396, 21–22.
610 Meeker, S.P., Bonnecaze, R.T., Cloitre, M., 2004a. Slip and Flow in Soft Particle
611 Pastes. Phys. Rev. Lett. 92, 198302.
612 https://doi.org/10.1103/PhysRevLett.92.198302
613 Meeker, S.P., Bonnecaze, R.T., Cloitre, M., 2004b. Slip and flow in pastes of soft
614 particles: Direct observation and rheology. J. Rheol. 48, 1295–1320.
615 https://doi.org/10.1122/1.1795171

Mooney, M., 1931. Explicit Formulas for Slip and Fluidity. J. Rheol. 1929-1932 2, 210–222. https://doi.org/10.1122/1.2116364

Ovarlez, G., 2011. Rhéologie des pâtes granulaires (thesis). Université Paris-Est.

Ovarlez, G., Chateau, X., 2008. Influence of shear stress applied during flow stoppage and rest period on the mechanical properties of thixotropic suspensions. Phys. Rev. E 77, 061403. https://doi.org/10.1103/PhysRevE.77.061403

Piau, J.M., 2007. Carbopol gels: Elastoviscoplastic and slippery glasses made of individual swollen sponges: Meso-and macroscopic properties, constitutive equations and scaling laws. J. Non-Newton. Fluid Mech. 144, 1–29.

Poumaere, A., Moyers-González, M., Castelain, C., Burghelea, T., 2014. Unsteady laminar flows of a Carbopol® gel in the presence of wall slip. J. Non-Newton. Fluid Mech. 205, 28–40. https://doi.org/10.1016/j.jnnfm.2014.01.003

Rabinowitsch, B., 1929. Über die viskosität und elastizität von solen. Z Phys Chem A 145, 1–26.

Russel, W.B., Grant, M.C., 2000. Distinguishing between dynamic yielding and wall slip in a weakly flocculated colloidal dispersion. Colloids Surf. Physicochem. Eng. Asp. 161, 271–282.

Salmon, J.-B., Bécu, L., Manneville, S., Colin, A., 2003. Towards local rheology of emulsions under Couette flow using Dynamic Light Scattering. Eur. Phys. J. E - Soft Matter 10, 209–221. https://doi.org/10.1140/epje/i2002-10110-5

638 Saramito, P., 2007. A new constitutive equation for elastoviscoplastic fluid flows.
639 J. Non-Newton. Fluid Mech. 145, 1–14.
640 https://doi.org/10.1016/j.jnnfm.2007.04.004
641 Servais, C., Ranc, H., Roberts, I. d., 2003. Determination of Chocolate Viscosity.
642 J. Texture Stud. 34, 467–497. https://doi.org/10.1111/j.1745-
643 4603.2003.tb01077.x
644 Sochi, T., 2011. Slip at Fluid-Solid Interface. Polym. Rev. 51, 309–340.
645 https://doi.org/10.1080/15583724.2011.615961
646 Sokmen, A., Gunes, G., 2006. Influence of some bulk sweeteners on rheological
647 properties of chocolate. LWT - Food Sci. Technol. 39, 1053–1058.
648 https://doi.org/10.1016/j.lwt.2006.03.002
649 Special Issue on Yield Stress Fluids: a 100 Years after Bingham's Landmark
650 Paper, 2017. . Rheological acta 56(3).
651 Steffe, J.F., 1996. Rheological Methods in Food Process Engineering. Freeman
652 Press.
653 Yeow, Y.L., Leong, Y.-K., Khan, A., 2006. Non-Newtonian flow in parallel-disk
654 viscometers in the presence of wall slip. J. Non-Newton. Fluid Mech. 139,
655 85–92. https://doi.org/10.1016/j.jnnfm.2006.07.005
656 Yilmazer, U., Kalyon, D.M., 1989. Slip Effects in Capillary and Parallel Disk
657 Torsional Flows of Highly Filled Suspensions. J. Rheol. 33, 1197–1212.
658 https://doi.org/10.1122/1.550049
659 Yoshimura, A., Prud'homme, R.K., 1988. Wall Slip Corrections for Couette and
660 Parallel Disk Viscometers. J. Rheol. 32.
661

List of Figure Captions

Fig.1: Apparent viscosity *vs* apparent shear rate evolutions at different times for the same molten chocolate sample measured with a 1mm gap smooth plate-plate. Solid dots (0min) represent the first increasing ramp. Open symbols: triangles (5min), diamonds (1h23min) and squares (2h41), represent decreasing ramps. The symbols show respectively steps number 1,2,6 and 10 of the proposed protocol.

Fig.2: Examples of apparent shear stress *vs* shear rates curves obtained at 1.50mm, 1.00mm, 0.75mm and 0.50 mm gaps.

Fig.3: (a) Schematic drawing of parallel plate-plate geometry. (b) Focus on the velocity field inside the geometry gap in the presence of slip at the solid wall.

Fig.4: Corrected shear stress versus apparent shear rate curves. The solid symbols are the mean values of interpolated data. The solid lines are the mean values of both the corrected and interpolated data. All experiments were carried out with a smooth plate-plate geometry at varying gap size: 1.8mm, 1.5mm, 1mm and 0.5 mm.

Fig.5: Apparent shear rate as a function of the reciprocal gap for different constant shear stresses. Details of each encountered behavior: (a) low shear rate: pure slip regime, (b) intermediate shear rate: transition regime (c) high shear rate: homogeneous bulk shear regime.

Fig.6: Apparent shear rate as a function of the reciprocal gap for different constant shear stresses represented by the solid lines. A summary of the different behaviors encountered on the left is symbolized by the three representations on the right: (a) at low shear rate (in green), a pure slip regime, (b) at intermediate shear rate (in red), a transition regime (c) at high shear rate (in blue), a homogeneous bulk shear regime.

Fig.7: Wall slip velocity as a function of the shear stress. The solid triangle symbols illustrate experimental data from the present work. The solid line represents the correspondingly best linear fit ($u_s = 4.55.10^{-3}\tau_R$). The open circle symbols represent the wall slip velocity evolution obtained using the *Yoshimura and Prud'homme* method with 0.50-0.75 mm; 0.50-1.50 and 1.00-1.50 mm gaps pair.

Fig.8: Evolution of the effective viscosity *vs* bulk shear rate. The solid line represents the present work's corrected data. Open circles represent the data obtained *via* the *Yoshimura and Prud'homme* method with 1.00-1.50mm; 0.50-1.50 and 0.50-0.75mm gaps pair.

Fig.9: Evolution of corrected shear stress *vs* bulk shear rate (solid circle symbols). The lines correspond to the different data fittings using *Casson* (in blue) and *Herschel-bulkley* (in orange) as models. Broken lines refer to the IOCCC standard conditions, *i.e.* a $2s^{-1}$-$50s^{-1}$ fitting while solid lines refer to a fit over the entire range of data, *i.e.* a 0.005-$50s^{-1}$ fitting.